

Finite Element Method Simulation and Multifactor Failure Analysis of an Important Stepped Shaft Fracture Events

First A. Qiu Jun

Senior Engineer
Shanghai Institute of Special Equipment
Inspection and Technical Research

Second B. Tong Yaoting

Engineer
Shanghai Institute of Special Equipment
Inspection and Technical Research

Third C. Ouyang Weiping

Engineer
Shanghai Institute of Special Equipment
Inspection and Technical Research

Aiming at a fracture event of an important stepped shaft parts, finite element method was used to simulate and analyze. Results show that the stress concentration is serious at the step and the maximum stress occurs at the transition corner, which exceeds the yield strength limit of the material under the most unfavorable condition. Scanning Electron Microscope and X-ray Energy Spectrum analysis shows that fracture of the shaft is a fatigue fracture initiated by multiple sources. Design analysis states that the initiation is mainly related to the small turning radius of the step, which caused stress concentration factor increase. Besides, the higher shoulder height caused sudden change of the section size and aggravated stress concentration effect. Furthermore, machining quality analysis indicates that the rough surface with micro-defects may be the origin of fatigue crack initiation. Heat Treatment process quality analysis indicates that improper control of quenching and tempering process had a negative impact on the initiation of crack. Working conditions analysis shows that the actual load state, which exceeded the design standard load spectrum, accelerated the fatigue damage.

Keywords: stepped shaft, fatigue fracture, finite element, failure analysis

1. INTRODUCTION

Finite Element Method (FEM) is a common method for the design and stress analysis of stepped axle, especially for stress concentration analysis[1-3]. In application of finite element method, mesh generation is a key step. Researchers need to select the appropriate mesh size according to the purpose of analysis [4-5]. In this paper, the finite element method is applied to fracture analysis of an important stepped shaft, while other failure analysis methods are synthesized, to find out the real cause of the fracture of the stepped shaft.

A 450t shipbuilding gantry crane in a company, which has been in operation for 3 years, is used in large lifting operation. Due to the breakage of the drum shaft of the lifting mechanism, the lifting objects fall to the ground and the crane is damaged.



Figure 1. Drum shaft of lifting mechanism of the crane

The fracture region was found locating at the step of the stepped shaft. By observing and analyzing extra features of the damaged area, investigators believed that the macro morphology of the section is fatigue fracture, and the final fracture zone is small (about 40mm).

2. GEOMETRY AND LOADING ANALYSIS OF SHAFT

Geometric sketch of the shaft was drawn, which shown that the fracture occurred at the turning corner of $\phi 180\text{mm}/\phi 220\text{mm}$ steps.

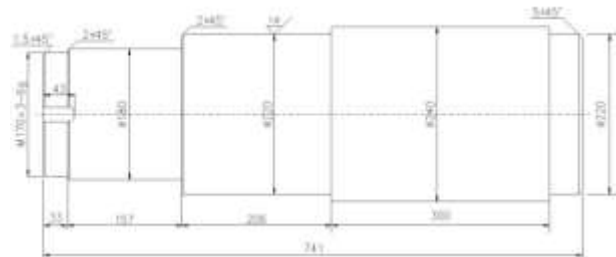


Figure 2. Geometric sketch of the shaft

According to the working conditions of the crane, the force analysis sketch of the drum structure was drawn, and the bearing support reaction of the drum shaft was solved, with the results shown in Table 1.

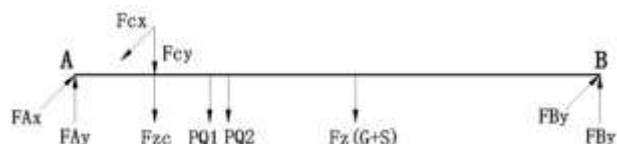


Figure 3. Diagram of force analysis of drum structure

Table 1. Bearing support reaction on drum shaft

F_{AX}	F_{AY}	F_{BX}	F_{BY}
242.1kN	682.2kN	14.7kN	141.3kN

3. FINITE ELEMENT SIMULATION

3.1 Model Establishment

The geometric model of the whole drum structure was established in CATIA.

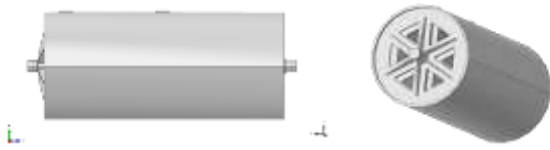


Figure 4. Geometric model of drum structure

As the fracture of the mechanism occurs on one side of the shaft only, so that it's unnecessary to apply the finite element analysis for the whole model. In finite element software ABAQUS, the drum part can be replaced by a through shaft ($D=240\text{mm}$), than both two ends of the mechanism can be connected together, thus the model can be easily calculated, while the bending moment and the force at the fracture will not change. The simplified model is shown in Figure 5.

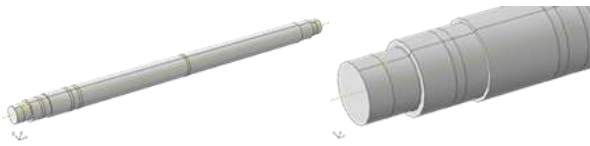


Figure 5. ABAQUS simplified finite element model

3.2 Material properties and constraints

The base material of the shaft is No.35 steel, whose Young's modulus is $212,000\text{MPa}$, Poisson's ratio is 0.31 , yield stress is 315MPa , and ultimate stress is 530MPa . The parameters are input into the material library of the finite element software, and the material properties are assigned to the components. As the hoisting mechanism used a self-aligning bearing, the shaft does not bear additional bending moment, so that the two fixed ends of the shaft are constrained by XYZ displacement in three directions, one end is constrained by YZ displacement in two directions, and the shaft is not constrained by rotation. The constraint diagram is shown in Figure 6.

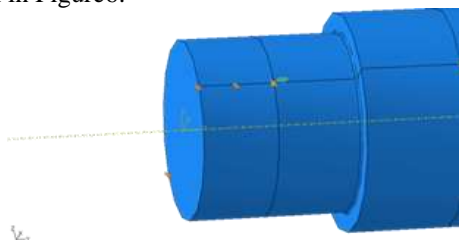


Figure 6. Constraint diagram of the model

3.3 Loading

Through analysis of the most unfavorable working conditions of the drum shaft, it can be concluded that the force acting on the drum single rope is X-direction $p=210.8\text{kN}$, and the tangential force, radial force and ring weight projected to the XZ plane respectively are, $F_{X1}=281.2\text{kN}$, $F_{Z1}=256.8\text{kN}$, and the total $F_{X2}=120.6\text{kN}$ of the drum and the wire rope on it. Due to the

singularity of stress in local area under concentrated load, the calculation results will be deviated. Therefore, the concentrated load is converted into volume force in the model, eliminating unnecessary errors caused by loading. The loading diagram is shown in Figure 7.



Figure 7. Load distribution of drum shaft

3.4 Finite Element Mesh

According to the size of the model and the requirement of calculation accuracy, entity unit and the mesh refinement was employed to the model, and the mesh is divided and refined at the corner transition of R2 (the mesh size set as 1.5mm). As the mesh size of different regions in the model varies greatly, tetra shaped elements was chosen.

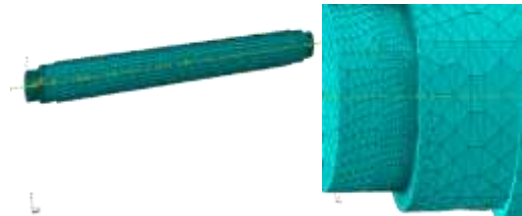


Figure 8. Model meshing and encryption

3.5 Results

After checking correctly, the model is submitted to ABAQUS software for post-processing calculation, and the calculation results are shown in Figure 9.

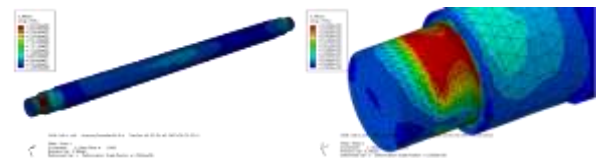


Figure 9. Stress distribution of the shaft and its left end

From Figure 9, it shows that the stress concentration occurs at the fracture site of the shaft under rated load. The stress distribution phase diagram of its left end is analyzed. Maximum stress occurs at the transition point of R2 fillet. The maximum stress value is 319.9MPa , which exceeds the yield strength limit of the material $R_{e1}=315\text{MPa}$. In order to stereoscopically reflect the stress state of this section, the section is cut off along R2 rounded cross section, XY plane and YZ plane, and the stress distribution diagram is shown in Figure 10.

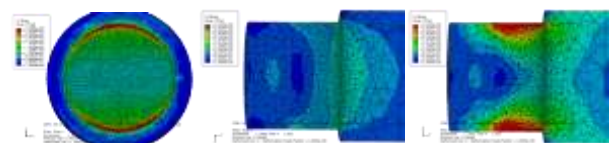


Figure 10. Stress distribution diagrams of cross section, xy section and yz section at R2 round corner at axis fracture

4. MULTIFATOR FAILURE ANALYSIS

4.1 Design Analysis of Shaft

The design structure diagram shows that the radius of transition corner $R=2\text{mm}$ at the step shaft $\phi 180\text{mm} / \phi 220\text{mm}$ is less than the national standard value, and it is quite different from the industry standard value. If the radius of transition corner is too small, the stress concentration factor will increase. The shoulder height is higher which cause the sudden change of the section size, and will aggravate the stress concentration effect.

4.2 Quality Analysis of Heat Treatment Process

According to the technical requirements of the shaft (35 steel), the hardness after quenching and tempering should reach 170HB-200HB. Brinell hardness was measured from surface to interior on longitudinal of the shaft at $\Phi 220\text{mm}$ fracture section. Physical and chemical test results show that the actual near surface hardness (220HB) exceeds the technical requirements, and the effective quenching layer depth is shallow, which has a certain impact on fatigue strength.

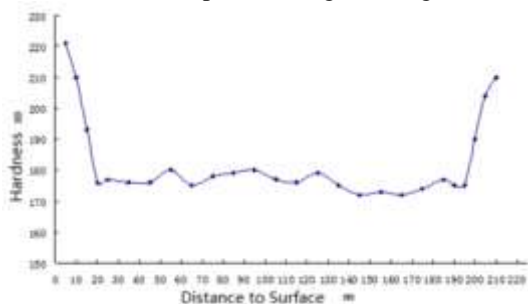


Figure 11. Hardness gradient on longitudinal section of shaft at $\Phi 220\text{mm}$ fracture zone

4.3 Quality Analysis of Metal Processing

There are obvious turning marks on the surface of the shaft near the fracture section. Compared with the roughness sample, the surface quality of the shaft is between $3.2\mu\text{m}$ and $6.3\mu\text{m}$, and the roughness of the surface does not meet the design requirement $Ra 1.6\mu\text{m}$. Surface state coefficient β has certain influence on fatigue fracture [6-7], and surface micro-defects may be the origin of fatigue crack initiation.

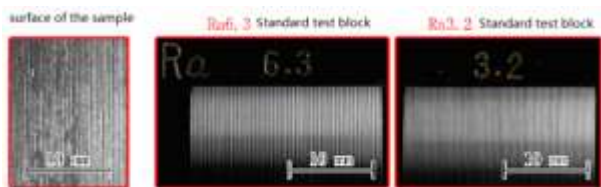


Figure 12. Comparisons of surface roughness in turning

4.4 Scanning Electron Microscope and X-ray Energy Spectrum Analysis

The fatigue fracture of shafting can be clearly confirmed by scanning electron microscopy (SEM) analysis of the fracture surface of shafting. On the outer surface of the shaft, there are rough bamboo-shaped metal processing marks and transverse stretch-like stripes with nodal spacing distribution; at higher

magnification, the morphology shows that the processing cracks open and turn, and extend to the edge of the section, which is related to the beginning of the section; at the edge of the section, there are parallel and dense fatigue stripes. Parallel fatigue growth fringes and intergranular secondary cracks can be seen in the sub-edge region, showing brittle morphology.



Figure 13. Machining traces of rough surface of axis and sub-layer fatigue glow

4.5 Working Conditions Analysis

Statistical data of hoisting mechanism operation show that the actual load state exceeds the L2-intermediate level of the design standard load spectrum, and it is easy to accelerate the fatigue damage of mechanical parts. At the same time, the fatigue fracture surface accounts for about 85% of the area of the cross-section, and the potential hazard cannot be found in daily use.

5. CONCLUSION

According to ABAQUS finite element simulation calculation, the maximum stress of local stress concentration exceeds the yield strength limit of material under the most unfavorable conditions at the transition corner of the shaft's $\phi 180\text{mm} / \phi 220\text{mm}$ step.

During the design of shaft, the selection of transition corner radius at fracture is too small and the selection of shoulder height is too large, which makes the stress concentration factor too high, and has adverse effects on the fatigue life of shaft.

The surface roughness and surface hardness of the fracture zone of the shaft do not meet the technical requirements, which will greatly reduce the toughness and fatigue resistance of the corner zone. The use beyond the design level has a negative impact on the initiation of cracking.

A large proportion of the fatigue growth zone on the cross section indicates that there is a period from crack initiation to final fracture, but the fatigue crack cannot be found in the daily maintenance of the crane during this period, which indicates that there is a blind area in the daily maintenance of the crane.

The fracture of the drum shaft is a fatigue fracture initiated by multiple sources. The initiation of the drum shaft is mainly related to the small transition fillet in the step area and the high stress concentration effect. It is easy to initiate fatigue cracking under impact load, which eventually leads to the overall failure, the drum losing its restraint, and high-speed rotation under the gravity drag of the suspender until the suspender falls to the ground and damaged.

ACKNOWLEDGMENT

This paper is support by The National Key Research and Development Program of China No.2017YFC0805705.

REFERENCES

- [1] Zhang J., Chen X.Y. and Wang L.. 2017 Journal of Anhui university of science and technology (natural science)37(3):56
- [2] Jiang B., Zhang Q. and Cui W.. 2018 Machine design and manufacturing engineering47(7):11
- [3] Liang K.S.2017Machinery55(10):67
- [4] Wang M.Q., Zhu Y.M. and Lu W.X.. 2004 Machinery design & manufacture 1:22
- [5] Wang Y., Lu L. and Li W.T.. 2014 Hoisting and conveying machinery3:52
- [6] Cai Y.. 2018 Internal combustion & parts21:128
- [7] Sun J.L., Jiang D.Z.. 2002 Journal of Yancheng institute of technology(natural science)15(4):21